Journal of CO_2 Utilization 39 (2020) 101175

Contents lists available at ScienceDirect

Journal of CO_2 Utilization

journal homepage: www.elsevier.com/locate/jcou

Are Fe based catalysts an upcoming alternative to Ni in CO_2 methanation at elevated pressure?

Tanja Franken[a,b,*], Andre Heel[a,c]

[a] Institute of Materials and Process Engineering, Zurich University of Applied Sciences — ZHAW, Technikumstrasse 9, CH-8401 Winterthur, Switzerland
[b] Paul Scherrer Institut PSI, Forschungsstrasse 111, CH-5232 Villigen PSI, Switzerland
[c] Institute of Environmental and Process Engineering (UMTEC), University of Applied Sciences Rapperswil (HSR), Oberseestr. 10, CH-8640 Rapperswil, Switzerland

ARTICLE INFO

Keywords:
High pressure methanation
Fe catalysts
Zeolite
CO_2 hydrogenation
High dispersion

ABSTRACT

The raise of regenerative but unsteadily produced energy demands a highly flexible way to store the energy for time periods when less energy is produced than consumed. In the current study, it is investigated if catalysts based on environmentally more attractive and less hazardous to health Fe might be able to be considered as an alternative to Ni catalysts in the CO_2 methanation at elevated pressure. For this a set of catalysts with 1–10 wt % Fe supported on the zeolite 13X is analysed in CO_2 methanation at 1–15 bar. The trends of activity as well as selectivity with varying Fe loading and pressure are presented. Correlation with thorough characterization of the materials shows that a very high dispersion of Fe in octahedral sites within the zeolite is necessary to generate CH_4 as the main reaction product and suppress the Fischer–Tropsch activity towards C—C coupling reactions at elevated pressure. Especially with low Fe loading such as 1 wt % high reaction rates of 42 mmol(CO_2)/(mol(Fe)·s) with a CH_4 selectivity of 76 % at 300 °C and 10 bar are obtained. In contrast to that, highly Fe loaded catalysts tend to form increasing amounts of Fischer–Tropsch products at increasing pressure. In addition, highly Fe-loaded catalysts are much more susceptible to destruction of the zeolite under reaction conditions. At the same time, highly loaded catalysts form a Fe_3C shell around the remaining support. Hence, avoiding the formation of a Fe_3C phase is crucial for high CH_4 selectivity. The results presented here therefore show that catalysts with a very high Fe-dispersion in particular can gain considerably in importance as alternatives to Ni-methanation catalysts at elevated pressure.

1. Introduction

Utilization of CO_2 is currently a hot topic in catalysis due to the chance to decrease anthropogenic CO_2 emissions on the one hand and to recycle it as a C_1 source in exchange to fossil fuels on the other hand. So called power-to-gas (PtG) and power-to-liquid (PtL) technologies enable chemical storage of surplus energy from regenerative sources by reaction of renewable H_2 with CO_2 to energy carrier such as methane (PtG) or liquid fuels (PtL) [1–3]. Especially the PtG technology has high potential as a chemical energy storage technology since infrastructure for fast energy generation as well as a natural gas grid based on fossil natural gas is already well established and a state-of-the-art-technology. Hence, renewably produced CH_4 via PtG can be easily feed into the existing gas grid and in a future perspective completely replace fossil natural gas.

Ni is the state of the art catalyst for CO_2 methanation (Eq. (1)) already since its discovery by Paul Sabatier in 1902 [4] and has been center of several studies on various supports, whereat reviews can be found elsewhere [1–3,5–14].

$$CO_2 + 4\,H_2 \rightarrow CH_4 + 2\,H_2O \quad (1)$$

Besides Ni, also other metals are active in CO_2 methanation [15,16]. Mills and Steffgen classified the important metals for methanation catalysts by its activity (Ru > Fe > Ni > Co > Mo) and selectivity to methane (Ni > Co > Fe > Ru) [17].

Ni shows high activity with a very good selectivity to CH_4. Nevertheless, traditional Ni-catalysts suffer from deactivation by sintering of the Ni particles upon heat evolution from the highly exothermic methanation reaction [18]. Deposition of coke and formation of volatile nickel carbonyls contribute to additional catalyst deactivation [19,20]. Besides, Ni is of toxicological concern. The sequences of Mills and Steffgen point out, that Fe has a very high activity for CO_2 activation but suffers from low selectivity. In contrast to Ni, iron is not toxic, is much more abundant and hence around 180 times cheaper

* Corresponding author at: Paul Scherrer Institut PSI, Forschungsstrasse 111, CH-5232 Villigen PSI, Switzerland.
E-mail address: tanja.franken@psi.ch (T. Franken).

https://doi.org/10.1016/j.jcou.2020.101175
Received 21 January 2020; Received in revised form 27 March 2020; Accepted 9 April 2020
Available online 24 April 2020

than nickel.

Surprisingly, only a few studies focus on optimization of Fe based catalysts for CO_2 methanation. Kirchner et al. investigated bare iron oxide samples in the CO_2 methanation and obtained best activity for nano-sized γ-Fe_2O_3 with maximum CH_4 yield of 60 % at 400 °C and ambient pressure [21]. In addition, pure α-Fe_2O_3 based catalysts can be promoted with 2 wt % Mg in order to increase the basicity and hence interaction of CO_2 with the catalysts. This promotion leads to improved CH_4 yield up to 32 % at 8 bar and a GHSV of 10,000 h^{-1} [22]. The results emphasize that the methanation takes place predominantly on surface carbon and iron carbide species on promoted bulk Fe_2O_3 catalysts [22]. In general, the high activity of Fe for CO_2 activation results from the high reverse-water-gas-shift (RWGS) activity (Eq. (2)) and especially at elevated pressure its further capability of CO hydrogenation via Fischer–Tropsch-Reaction (FTR) (Eq. (3)).

$$CO_2 + H_2 \rightarrow CO + H_2O \quad (2)$$

$$nCO + m/2n + 1\ H_2 \rightarrow 1/n\ C_nH_m + n\ H_2O \quad (3)$$

Lee et al. investigated the CO_2 hydrogenation via FTR on Fe catalysts at 1–25 bar and in various H_2/CO_2 ratios [23]. They found that metallic Fe transforms into mixtures of magnetite and carbides under reaction conditions. Especially in the pressure range of 1–10 bar the increase of pressure leads to an increase of the chain length and higher temperature increases the CO_2 conversion as well as CO and CH_4 yield. In contrast, the produced H_2O from FTR contributes to the equilibrium of the RWGS-reaction that limits the CO_2 conversion [23]. In line, on K and S promoted Fe-based catalysts it was shown that the CO_2 methanation activity is strongly influenced by the H_2/H_2O ratio effluent from the reactor [24,25]. It was claimed that conversions increase with increasing H_2/CO_2 ratio and cannot be further improved than their maximum CO_2 conversion of 44 % obtained at 20 bar and a H_2/CO_2 ratio of 8 [24].

With the aim of tailoring Fe-based materials as CO_2 methanation catalysts, studies on increasing the C_2–C_4 fraction in CO-FTR, with CH_4 as an undesirable product, provide information on the direction of necessary properties for high CH_4 yields: In general, iron carbides are considered as the active phase in FTR and active carbon sites contribute to the chain growth mechanism [26]. In addition, the activity and selectivity is closely related to the particle size of the Fe-based catalysts [26]. Smaller Fe nanoparticles (< 7–9 nm) lead to higher CH_4 selectivity [27–29]. It was concluded, that low coordinatively unsaturated corner and edge sites are important for CH_4 formation, while terrace sites of the bigger Fe particles are responsible for olefin generation [29,30]. Hence, the selectivity of Fe based catalysts for CO_2 methanation could be improved by decreasing the Fe particle size. This stands in contrast to the particle size dependency of Ni based CO_2 methanation catalysts, which decrease in selectivity if the particle size decrease below 2 nm [31,32].

Supporting Fe on zeolites enables a way to produce stable and highly dispersed Fe species. This has been proven by their use as highly stable selective catalytic reduction (SCR) catalysts [33–35]. Despite the high Fe dispersion, zeolites offer additional tailoring possibilities and have shown to positively influence the CO_2 methanation performance of Ni-based catalysts [36]. Namely by their compensating cation [37], Si/Al ratio [38] and zeolite framework type such as FAU, BEA, MFI and MOR [39]. Due to the high affinity of zeolites to adsorb water they allow further improvement of catalytic activity by applying so called sorption enhanced conditions whereat H_2O is adsorbed by the zeolite and in that way pulled away from the reaction center [40–44]. To the best or our knowledge it was not investigated yet how the combination of Fe supported on zeolites perform in CO_2 methanation. In the present study a series of differently loaded Fe on zeolite catalysts are investigated at ambient and elevated pressure up to 15 bar with the aim to increase the CO_2 methanation performance. In order to avoid restricting the product spectrum resulting from pore size effects within the zeolite, 13X was selected as zeolite support. On the one hand due to its relatively large and three dimensional pore structure where molecules up to a kinetic diameter of 7.35 Å can form and diffuse freely along all axis including CO, CH_4, CH_3OH as well as C–C coupled products up to at least C_6 compounds. On the other hand a large range of Fe loadings can be theoretically ion exchanged due to the high aluminium content of 13X. As main focus the trends in activity and selectivity with increasing pressure as well as iron loading are carefully analysed and correlated with the properties of the catalysts. This leads to a justification if CO_2 methanation on Fe-based catalyst will become feasible as an attractive alternative.

2. Experimental

2.1. Catalyst preparation — synthesis of Fe/13X

1, 5 and 10 wt % Fe/13X catalysts were synthesised by wet impregnation with a 0.05 M $Fe(NO_3)_3 \cdot 9H_2O$ (99 % Sigma-Aldrich) solution in ethanol on commercial Na-13X zeolite (ZEOCHEM, Si/Al = 2.5; Faujasite structure). After ion exchange for 24 h at room temperature under intense stirring ethanol was evaporated in a rotary evaporator. The resulting solids were dried at 80 °C for 12 h and calcined at 400 °C (heating ramp = 5 K/min) for 5 h in a continuous flow of air. The 5 wt % catalyst with collapsed zeolite structure was synthesised by wet impregnation for 30 min with a 0.05 M $Fe(NO_3)_3 \cdot 9H_2O$ aqueous solution on commercial Na-13X. Water was evaporated in a rotary evaporator, the resulting solid dried at 80 °C for 12 h and calcined at 500 °C (heating ramp 5 K/min) for 5 h in a flow of air.

2.2. Catalyst characterization

The weight loadings of iron of all samples were analysed via Inductively Coupled Plasma Optical Emission Spectroscopy (ICP-OES) on an Agilent 720 ES. The X-ray powder diffraction pattern were measured on a Bruker D8 Advance diffractometer with Ni filtered Cu K_α radiation (λ = 1.5406 Å) and a step size of 0.2° from $2^\circ\theta$ = 20–90. Crystallite sizes of the Fe-particles were calculated according the Debeye–Scherrer equation using the half width of the reflex at 44.7°. UV/vis spectra were collected on a UVVISNIR Lambda 950 spectrometer from Perkin Elmer equipped with a 150 mm integration sphere to analyse the diffuse reflectance of the Fe-zeolites. The spectra where recorded in reflexion mode in a wavelength region of 800–200 nm and a step size of 5 nm. Specific surface area, pore diameter and pore diameter dispersion were analysed by N_2 physisorption at 77 K in a Quantachrome Autosorb IQ TPX. All samples were degassed for 12 h in vacuum at 200 °C. The pore diameter and dispersion were analysed according the BJH method from the desorption branch and specific surface area (SSA) by using the BET method. The pressure range for analysis was defined by rouquerol analysis in order to stay in the linear regime of the BET analysis [45]. The microporous surface area was distinguished from the external and mesoporous surface area by the t-plot method. Temperature controlled analysis were performed in the same Quantachrome Autosorb IQ TPX in dynamic mode and with a thermal conductivity detector. For temperature programmed reduction (H_2-TPR) all samples were degassed at 400 °C in a flow of N_2 for 30 min. Subsequent to the cooling down procedure to 40 °C, TPR was started in a flow of 5 vol% H_2 in N_2, with a total flow rate of 25 mL/min and a heating ramp of 5 K/min up to 850 °C and isothermally treated at the end temperature for additional 30 min. NH_3 was used in order to analyse the acidic properties of the zeolite in the temperature controlled desorption (TPD) experiments. Prior to the analysis all samples were reduced in a flow of 50 % H_2 in N_2 at 400 °C for 30 min, accordingly to the pre-treatment of the catalytic tests. Residual adsorbed hydrogen was flushed-off from the samples by additional 2 h treatment in N_2 at 400 °C. Subsequently, adsorption of 10 % NH_3 in N_2 was performed at 100 °C and physisorbed NH_3 was purged in a flow of N_2 at 100 °C for

30 min. TPD was performed in a flow of 25 mL/min N_2 and a heating ramp of 10 K/min up to 800 °C. Scanning electron microscopy (SEM) analysis was performed in a Thermo Scientific Phenom XL equipped with a back scattered detector. Concurrent elemental mapping was carried out by using the integrated EDX detector.

2.3. Catalytic tests

Methanation tests were performed in fixed bed flow reactor system with an inner diameter of 6 mm at ambient and elevated pressure (5, 10, 15 bar) at a GHSV = 4186 h^{-1}. Prior to the catalytic tests all catalysts were reduced within the reactor in a flow of 50 % H_2 in N_2 for 30 min at 400 °C and ambient pressure. In a typical run 25 mL/min CO_2, 100 mL/min H_2 and 12 mL/min N_2 as internal standard were supplied by mass flow controller (Bronkhorst, El Flow). During the methanation tests the temperature was raised from 200 to 400 °C in steps of 50 °C and kept constant at reaction temperature for 30 min. The composition of effluent gases from the reactor was monitored by online raman spectroscopy (Kaiser Raman RXN2 spectrometer equipped with AirHead probes). The conversion X, selectivity S and reaction rate of CO_2 conversion (r(CO_2)) were calculated according Eqs. (4)–(6):

$$X(CO_2) = \frac{\dot{n}(CO_{2\,in}) - \dot{n}(CO_{2\,out})}{\dot{n}(CO_{2in})} \quad (4)$$

$$S(CH_4) = \frac{\dot{n}(CH_{4\,out})}{\sum \dot{n}\,(products)} \quad (5)$$

$$r(CO_2) = \frac{X(CO_2) \times \dot{n}(CO_2)}{n(Fe_{cat})} \quad (6)$$

With $\dot{n}_i$ as the molar flow of component i, and n(Fe_{cat}) as the molar amount of Fe in the catalyst bed within the reactor.

3. Results and discussion

3.1. Characterization

Catalysts with three different weight loadings (1, 5, 10 wt %) of Fe on 13X were prepared via impregnation. Elemental analysis via ICP-OES confirms the presence of Fe on 13X close to the aimed amounts of Fe on the samples (Table 1).

Since the zeolite framework is prone to destruction by iron, the integrity of the structure was validated via XRD analysis.

The impregnation procedure and calcination temperature strongly influences the stability of the iron impregnated zeolites. Hence, a synthesis optimization was conducted: the zeolite structure stays intact only by avoiding H_2O as a solvent and using ethanol as well as decreasing the calcination temperature to 400 °C (Fig. 1). Nevertheless, with higher Fe-loading the decrease of intensity of reflexes shows the incipient destruction of the framework even by applying the optimized procedure. Compared to the pure 13X, 1 wt % Fe/13X shows nearly no changes in intensity and all catalysts show reasonable stability. In contrast, the zeolite structure of 5 wt % Fe/13X impregnated in H_2O and calcined at 500 °C completely vanishes. For this reason, all catalysts were prepared in ethanol and by calcination at 400 °C and it was avoided to exceed this temperature at any time. As a pretreatment in the catalytic test a reduction of the catalysts in 50 % H_2 in N_2 at 400 °C for 30 min was performed. Comparison of XRD of *ex situ* reduced and as calcined catalysts (Fig. 1) ensure that the zeolite structure stays intact for all Fe loadings during the pre-reduction and confirm the Fe-reduction by the raise of the specific reflex of metallic Fe at 2°θ of 44.7° (inset in Fig. 1). According to the Debeye–Scherrer equation extracted Fe crystallite sizes from this reflex are 33 and 23 nm for 5 wt % and 10 wt % Fe/13X, respectively. Solely the reduced 1 wt % Fe/13X does not show this specific reflex. This could be due to two reasons, or a combination thereof: Either the Fe loading is too low for the sensitivity of XRD or the Fe species are highly dispersed within the framework of the zeolite.

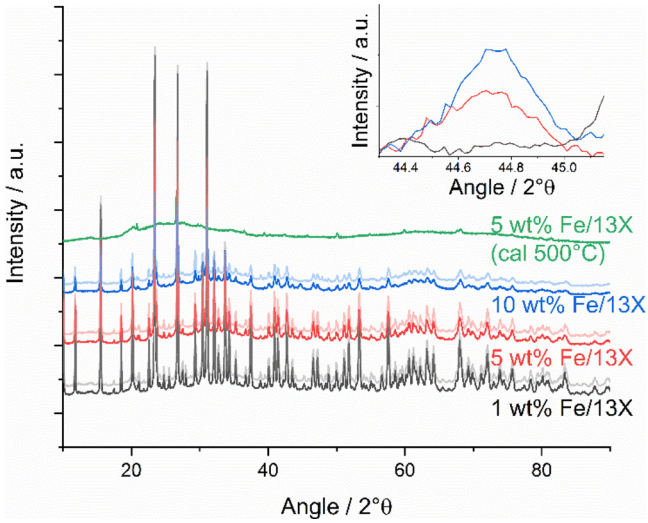

Fig. 1. X-ray diffractograms of reduced (400 °C) 1, 5 and 10 wt % Fe/13X catalysts and comparison to 5wt % Fe/13X prepared in H_2O and calcination at 500 °C (green) (light colours: corresponding as calcined catalysts) Inset: indication of the raise of metallic Fe reflex with increasing Fe loading after reduction.

N_2 physisorption analysis confirms the presence of microporosity of all Fe/13X catalysts calcined at 400 °C. Nevertheless, the specific surface area decreases from 612 to 161 m^2/g with increasing Fe loading. In line with the decreasing reflex intensity of the zeolite lattice from XRD analysis the micropore area extracted from t-plot analysis decreases from 573 down to 32 m^2/g (see Table 1).

The dispersion of Fe within the zeolite framework after calcination was analysed with UV/vis spectroscopy. The line shape of the spectra arising from O → Fe^{3+} charge transfer are rather similar (Fig. 2). In all spectra, four distinct peaks are separated by deconvolution (Figs. S1–S3). Two strong bands are found below 300 nm that are assigned to isolated Fe^{3+} ions. Whereat the band centered at 205 nm attributes to charge transfer from tetrahedral coordinated Fe^{3+} and the band at 250 nm relates to Fe^{3+} in higher coordination [34]. The two bands above 300 nm arise from agglomerated Fe-species. Whereby the band from octahedral Fe^{3+} species in small oligomeric Fe_xO_y cluster appears at 350 nm and from large Fe oxide particles as a very broad band at 436 nm. Quantitative analysis of the deconvoluted bands shows that all samples have the same relative amount of Fe^{3+} in tetrahedral sites. Contrary to this, 1 wt % Fe 13X shows with 55 % of all Fe^{3+} ions relatively more Fe ions in dispersed and oligomeric octahedral sites. Solely 30 % of the Fe ions agglomerate to particles. In comparison to this, the two higher loaded samples have comparable factional amounts of Fe in all sites and more than 55 % of Fe agglomerate into particles.

The reducibility of the Fe/13X catalysts was investigated by H_2TPR experiments (Fig. 3). In line with the Fe loading of catalyst the intensity

Table 1
Overview of physicochemical properties: weight loading of Fe from ICP-OES, specific surface area (SSA), pore half width (r(pore)), micropore area (S(micro)) derived from N_2 physisorption and Fe crystallite size from XRD.

Sample	wt % Fe	SSA [m^2/g]	r(pore) [Å]	S(micro) [m^2/g]	D(cryst) [nm]
1 wt % Fe/13X	1.3	612	4.12	573	–
5 wt % Fe/13X	4.6	423	4.32	278	33
10 wt % Fe/13X	8.2	161	19.13	32	23

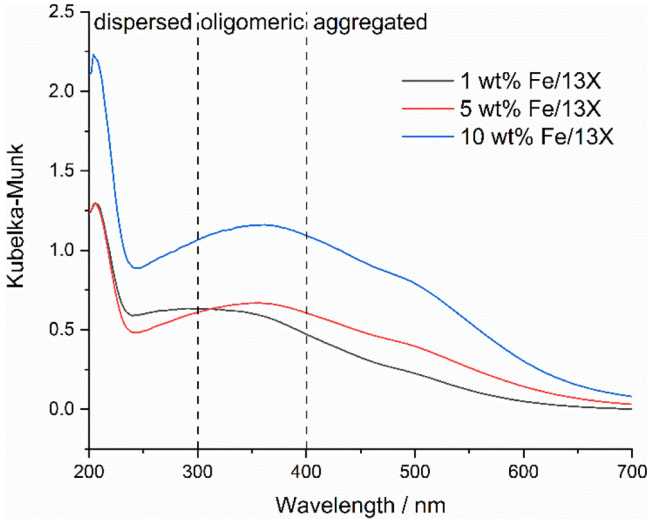

Fig. 2. Diffuse reflectance UV/vis spectra of 1–10 wt % Fe/13X catalysts after calcination. Individual deconvoluted spectra can be found in the supporting information.

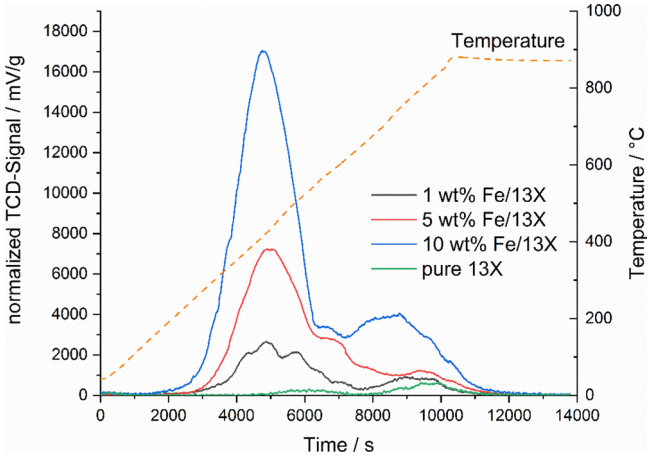

Fig. 3. TPR profiles of 1–10 wt % Fe impregnated on 13X zeolites.

of the signals increases and the features of 5 and 10 wt % Fe/13X samples are rather similar. These two samples show a very intense and broad signal between 200–550 °C with a peak maximum that shifts to lower temperatures from 442 to 405 °C with increasing Fe loading from 5 to 10 wt %. In agreement with literature these signals correspond to the reduction of Fe of the agglomerated FeO_x particles and dominate the TPR [46]. In addition, two more signals appear at temperatures higher than 550 °C that go in line with the collapse of the zeolite structure.

In the TPR of 1 wt % Fe/13X three distinct peaks appear in the temperature region of zeolite's thermal stability with peak maxima at 375, 424 and 498 °C. According to literature, reduction of Fe^{3+} within the zeolite structures as well as reduction of Fe_2O_3 to Fe_3O_4 from oligomeric and small cluster takes place at lower temperature [47]. The visibility of the fine structure of reduction under the same measurement conditions shows on the one hand that agglomerated FeO_x-species are not the main species, and on the other hand, that Fe species coordinated on different sites of the zeolite framework are present in this sample.

Temperature programmed desorption of NH_3 was performed in order to analyse the influence of the Fe loading on the zeolites acidity (Fig. S4). In line with the decrease of reflex intensity of the zeolite framework in the XRD with increasing Fe loading the total number of acid sites decreases. The main signal in the TPD appear at the same temperature region. Hence, even though the number of acid sites

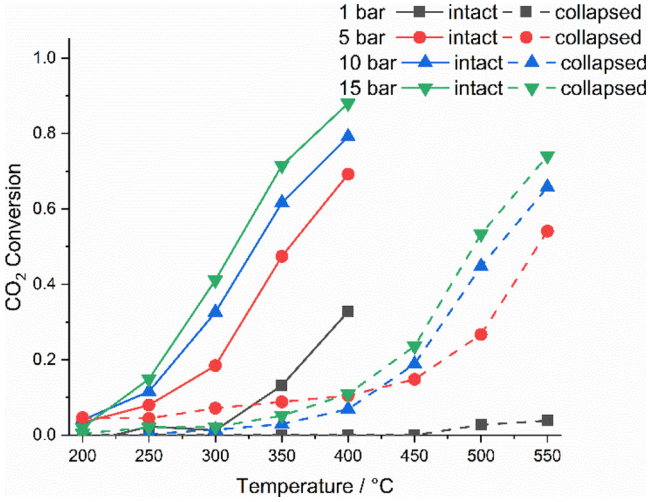

Fig. 4. CO_2 conversion at increasing temperature and pressure on 5 wt % Fe/13X with collapsed (broken lines) and intact (solid lines) zeolite structure. Reaction conditions: GHSV = 4186 h^{-1}, V(gas) = 137 mL/min, H_2/CO_2 = 4/1.

decreases with increasing Fe load, the acid strength as well as nature of acid sites remain constant in all samples. Therefore, it can be excluded to significantly influence the selectivity of the catalysts.

3.2. Catalytic tests

3.2.1. Influence of availability of zeolite framework on CO_2 conversion

All prepared materials were investigated in a temperature region of 200–400 °C and at pressures of 1, 5, 10 and 15 bar.

In a first step the two 5 wt % Fe/13X with a collapsed (prepared in H_2O and calcined at 500 °C, broken lines in Fig. 4) and intact zeolite structure (calcined at 400 °C & exclusion of H_2O from the synthesis, solid lines in Fig. 4) were compared by their catalytic performances. In case of the catalysts with a collapsed framework after synthesis a rather low CO_2 conversion of 10 % was observed by increasing the temperature up to 400 °C, even at 15 bar. For this reason, the temperature range of the catalytic test was expanded to 550 °C for this catalyst. At 1 bar no significant CO_2 conversion was observed up to 550 °C. Likewise all other investigated catalysts, the CO_2 conversion increases with temperature and increasing pressure of the catalytic tests. With 5 wt % Fe on collapsed 13X reasonable CO_2 conversion was achieved up to 74 % at 550 °C and 15 bar. On this catalyst, CO is the main product at low pressure. With increasing pressure, selectivity towards CH_4 increases up to 85 % at 15 bar and 550 °C. No Fischer–Tropsch products were observed under any conditions.

On the contrary, 5 wt % Fe/13X with an intact zeolite framework shows already reasonable CO_2 conversion of 33 % at 1 bar and 400 °C. CO_2 conversion increases with temperature and pressure up to 88 % at 400 °C and 15 bar. Incipient activity is already obtained at 250 °C. Hence, the comparison of these two catalysts clearly demonstrates that an intact zeolite framework is essential to obtain and support high catalytic performances at reasonable temperatures.

3.2.2. Influence of pressure and Fe-loading on reaction rates

In order to stay in the kinetic regime the Fe-normalized reaction rates at 300 °C are used to compare the activity of produced catalysts with intact zeolite structure and different Fe loading at pressures from 1 to 15 bar (Fig. 5). The catalyst masses included in the reactor and corresponding Fe-content from ICP analysis were used to calculate the Fe molar reaction rates. The two catalysts with 5 and 10 wt % Fe/13X show similar and increasing reaction rates at increasing pressure of up to 12 and 8 mmol(CO_2)/(mol(Fe)·s), respectively. This points out that the main active sites are the same in these two catalysts. In opposition

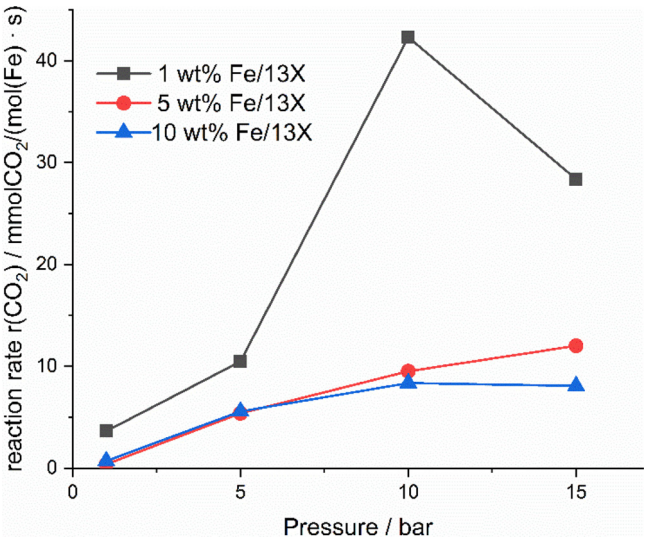

Fig. 5. Variation of CO_2 reaction rate with increasing pressure on 1, 5, 10 wt % Fe/13X at 300 °C. Reaction conditions: GHSV = 4186 h^{-1}, V(gas) = 137 mL/min, H_2/CO_2 = 4/1.

to these results, 1 wt % Fe/13X shows much higher reaction rates at all investigated pressures up to 42 mmol(CO_2)/(mol(Fe)·s) at 10 bar. These trends show in correlation to the UV/vis analysis that finely dispersed Fe-species, which are the main species in 1 wt % Fe/13X, have a much higher catalytic activity than the agglomerated Fe-species, that are the main species of the 5 and 10 wt % loaded Fe/13X catalysts. Nevertheless, the reaction rate decreases upon further increase of the pressure from 10 to 15 bar against the principle of Le Chatelier. This might be either due to hampered desorption of one of the products from the catalyst surface or reconstruction of the Fe-species or zeolite framework at elevated pressure.

The catalytic performances at 350 °C are used to compare the variation of product selectivity of different Fe loading and at varying pressures (Fig. 6).

At 1 bar the 10 wt % Fe/13X catalyst shows a very high selectivity towards CO (S(CO) = 97 %) and minor selectivity to CH_4 (Fig. 6a). With increasing pressure to 15 bar the selectivity towards C–C coupled products and CH_4 increases monotonously. CH_4 becomes the main product at 10 bar and reaches its maximum selectivity of 61 % at 15 bar. The selectivity to C–C-coupled products increases up to 22 %, while the selectivity towards CO decreases to 15 %.

Likewise, 5 wt % Fe/13X catalyst shows the same trend with increasing pressure (Fig. 6b). At high pressures it increases its selectivity towards the desired product CH_4 up to 68 %, while the selectivity towards CO (S(CO) = 14 %) and CC-coupled products (S(CC) = 17 %) stays relatively low.

In contrast to the behavior of the two higher loaded Fe catalysts 1 wt % Fe/13X shows at 1 bar already significant CH_4 selectivity of 22 % (Fig. 6c). The CO selectivity of 21 % at 350 °C and 1 bar is relatively low and selectivity towards C–C coupled products is at 56 % and therefore surprisingly high in that sequence. In opposition to the trend of 5 and 10 wt % Fe/13X as well as literature [26] on Fe-based Fischer–Tropsch catalysts, the selectivity towards C–C-coupled products decreases with increasing pressure on 1 wt % Fe/13X. The main product is CH_4 from 5 to 15 bar with a selectivity up to 76 % at 10 bar and 350 °C. Comparable product selectivites of S(CO) = 11 % and S(CC) = 14 % are observed at 10 and 15 bar. This trend of decreasing selectivity towards C–C coupled products and increasing CH_4 selectivity with increasing pressure is opposed to the general trend of Fe-based Fisher–Tropsch catalysts reported in literature [26], in which Fe_3C is regarded as active species. But it stands in line, that more coordinative unsaturated Fe species have a higher tendency to produce CH_4 [29,30].

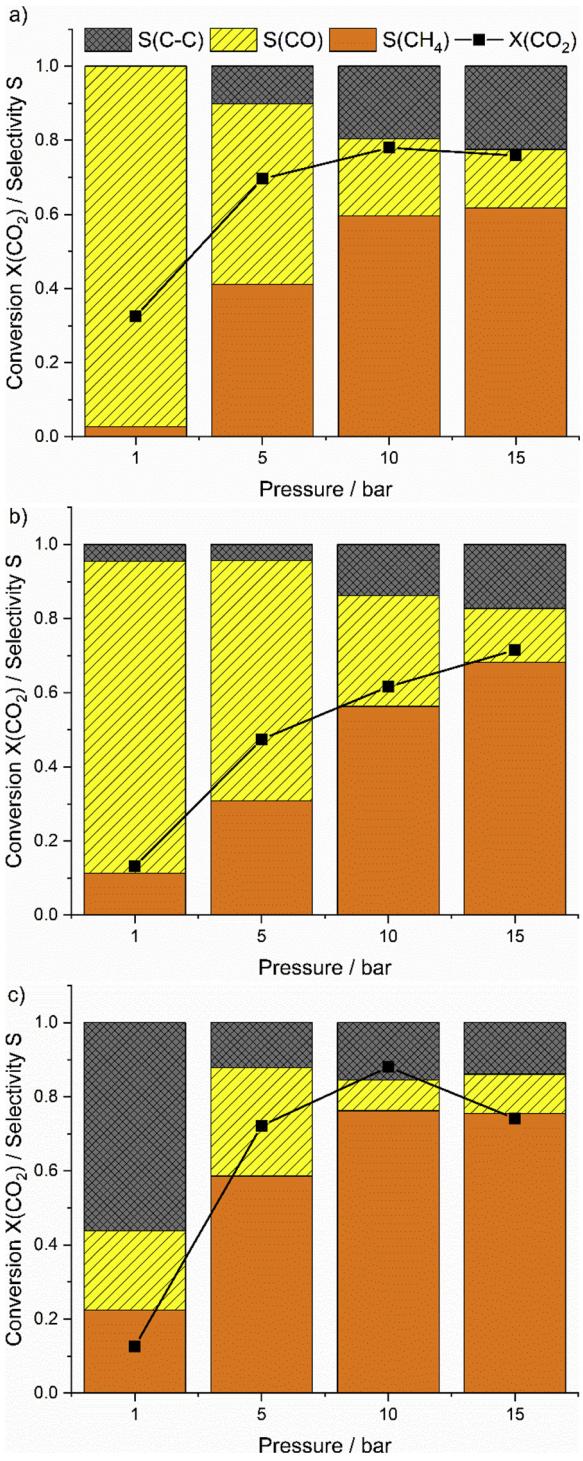

Fig. 6. Variation of product selectivity with pressure for (a) 10 wt % Fe/13X; (b) 5 wt % Fe/13X and (c) 1 wt % Fe/13X. Reaction conditions: GHSV = 4186 h^{-1}, V(gas) = 137 mL/min, H_2/CO_2 = 4/1; T = 350 °C.

XRD analysis of the catalyst after the catalytic tests shows a decrease of the reflexes from the zeolite framework for all samples (Fig. 7). Nevertheless, 1 wt % Fe/13X shows considerably high intensities. Hence, the integrity of the framework is still given in the mayor fraction of the sample even though a small fraction of the zeolite framework collapses. In the XRD of this sample no other reflexes from other phases than the 13X framework are visible. In contrast to the results of 1 wt % Fe catalysts 5 and 10 wt % Fe catalyst show significant decrease and a full depletion of the reflexes from the zeolite. Additionally, reflexes

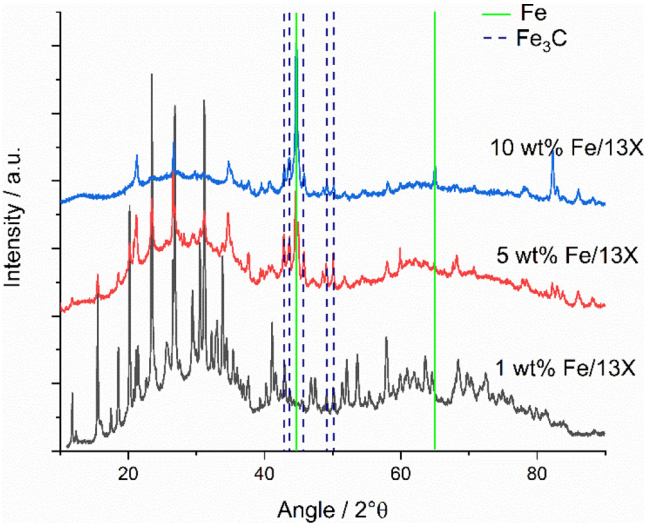

Fig. 7. XRD analysis of the used catalysts after catalytic testing.

from a Fe_3C phase appear in the diffractograms of both catalysts after the methanation experiments. Given by the sharp shape of metallic Fe reflex in the 5 and 10 wt % Fe/13X catalysts the crystallite size of Fe increases during the catalysis. On the low loaded 1 wt % Fe/13X still no reflexes origin from metallic Fe or Fe_3C, respectively, under reaction conditions. Hence, the included Fe is very stable within the framework of the zeolite.

The collapse of the zeolite with high Fe loading is visible in the SEM micrographs as well. The spherical shape of the zeolite crystallites is still visible in the used 5 wt % Fe/13X catalysts (Fig. S5). This shape nearly vanishes completely on the 10 wt % Fe/13X catalyst after operation. Larger fragments with different morphology, consisting of Al and Si, become obvious instead (Fig. 8 bottom, middle & right). In addition to this, the formation of larger Fe particles is visible, too. In comparison to SEM images of the reduced catalysts prior to the catalytic testing it seems that Fe migrates out of the zeolite particles and forms, together with deposited carbon, an outer shell around the support (Fig. 8 bottom). In the case of the used 10 wt % Fe/13X catalyst the EDX mapping indicates that residual zeolite particles do not contain Fe at all, while the concentration of Fe is comparably high on the amorphous fragments (Fig. 8). As opposed to this the spherical shape of the 1 wt % Fe/13X zeolite catalyst particles appears to be unchanged after the reaction in the SEM micrographs (Fig. 8 top). In addition, EDX analysis shows a homogeneous dispersion of Fe over the sample and no larger particle agglomerations of Fe or creation of a common Fe–C shell/layer is visible. Hence, the SEM micrographs confirm together with XRD analysis the destruction of the higher loaded zeolite during the catalytic run under formation of a Fe_3C shell at the outer layer of the catalysts.

4. Conclusions

The hydrogenation of CO_2 towards CH_4 on differently loaded Fe/13X catalysts was investigated at ambient and elevated pressure (5–15 bar). Comparison of the catalytic performances with a catalyst with collapsed zeolite framework shows, that an intact zeolite structure and hence high dispersion of Fe within the catalyst is essential for high CO_2 conversion at temperatures below 400 °C and all investigated pressures.

Catalytic tests on 10, 5 and 1 wt % Fe/13X catalysts with intact

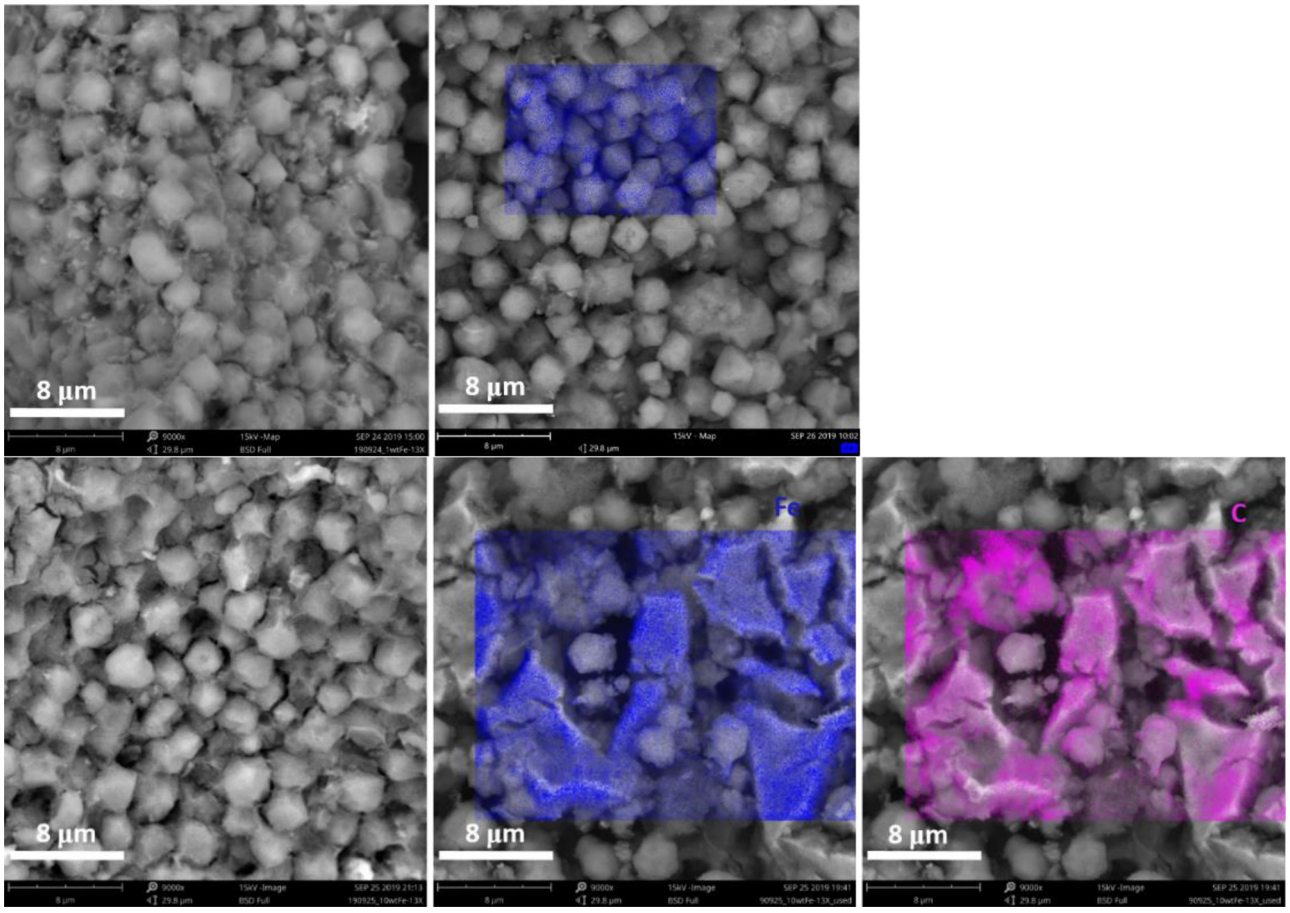

Fig. 8. SEM analysis of reduced (left) and used (centre & right) 1 wt % Fe/13X (top) and 10 wt % Fe/13X (bottom).

zeolite structure revealed a different reactivity of the two higher loaded catalysts compared to the 1 wt % Fe/13X catalyst. Higher Fe-loading leads to relatively low reaction rates of up to 12 mmol(CO_2)/(mol(Fe)·s) at 15 bar. CO is the main reaction product at low pressures of 1 and 5 bar. With increasing pressure the selectivity towards CH_4 as well as C–C-coupled products increases. The low Fe-loading of 1 wt % leads to a significant increase of the molar reaction rate at all investigated pressures up to 42 mmol(CO_2)/(mol(Fe)·s) at 300 °C and 10 bar. In contrast to both higher Fe-loadings, the lower Fe-loading leads to high selectivity for C–C-coupled products of 56 % at 1 bar. The selectivity towards desired CH_4 increases up to 76 % with increasing pressure at the expenses of the formation of CO and C–C-coupled products.

Physico-chemical characterization before and after the catalytic run show on the one hand that in 5 and 10 wt % Fe catalysts, Fe is mainly present as agglomerated particles. This leads to a destabilization of the zeolite and further agglomeration of Fe under reaction conditions with simultaneous formation of Fe particles embedded in a Fe_3C-phase as an outer shell layer. On the other hand, in 1 wt % Fe/13X, Fe is mainly present as octahedrally coordinated dispersed and oligomeric species. This leads to a higher hydrothermal stability of the catalysts and neither formation of larger Fe agglomerates nor Fe_3C-phase formation under operation. The high dispersion of Fe within the material suppresses C—C coupling reactions at higher pressure due to confined neighboring Fe sites and this in turn supports the hydrogenation of CO_2 to methane. At 15 bar the selectivity towards CO is limited down to 8 %. Even though the performance is not yet fully optimized, the presented results show, that the utilization of Fe-based catalysts as alternative to more expensive and especially hazardous Ni-catalysts for e.g. biogas upgrading and feed into the natural gas grid becomes considerable and provides essential prerequisites for the direction of further catalyst optimization.

Declaration of competing interests

The authors declare that they have no known competing financial interests or personal relationships that could have appeared to influence the work reported in this paper.

CRediT authorship contribution statement

Tanja Franken: Conceptualization, Methodology, Validation, Formal analysis, Investigation, Writing - original draft, Writing - review & editing, Visualization, Project administration, Funding acquisition. **Andre Heel:** Conceptualization, Methodology, Writing - review & editing, Supervision, Project administration, Funding acquisition.

Acknowledgements

The authors kindly acknowledge funding of the SmartHiFe Project by the Swiss Federal Office of Energy (grant number: SI/501754-01). Additionally the authors kindly thank Michal Gorbar and Dr. Roman Kontic for their support during the SEM and XRD analyses.

Appendix A. Supplementary data

Supplementary material related to this article can be found, in the online version, at doi:https://doi.org/10.1016/j.jcou.2020.101175.

References

[1] T. Weitzel, C.H. Glock, Energy management for stationary electric energy storage systems: a systematic literature review, Eur. J. Oper. Res. 264 (2018) 582–606, https://doi.org/10.1016/j.ejor.2017.06.052.
[2] H. Chen, T.N. Cong, W. Yang, C. Tan, Y. Li, Y. Ding, Progress in electrical energy storage system: a critical review, Prog. Nat. Sci. 19 (2009) 291–312, https://doi.org/10.1016/j.pnsc.2008.07.014.
[3] S. Saeidi, N.A.S. Amin, M.R. Rahimpour, Hydrogenation of CO_2 to value-added products — a review and potential future developments, J. CO_2 Util. 5 (2014) 66–81, https://doi.org/10.1016/j.jcou.2013.12.005.
[4] J.-B. Senderens, P. Sabatier, Nouvelles du synthèses du méthane, C. R. Acad. Sci. 82 (1902) 514–516.
[5] X. Su, J. Xu, B. Liang, H. Duan, B. Hou, Y. Huang, Catalytic carbon dioxide hydrogenation to methane: a review of recent studies, J. Energy Chem. 25 (2016) 553–565, https://doi.org/10.1016/j.jechem.2016.03.009.
[6] M. Aresta, A. Dibenedetto, Utilisation of CO_2 as a chemical feedstock: opportunities and challenges, Dalton Trans. (2007) 2975–2992, https://doi.org/10.1039/b700658f.
[7] M. Aresta, A. Dibenedetto, E. Quaranta, State of the art and perspectives in catalytic processes for CO_2 conversion into chemicals and fuels: the distinctive contribution of chemical catalysis and biotechnology, J. Catal. 343 (2016) 2–45, https://doi.org/10.1016/j.jcat.2016.04.003.
[8] W. Li, H. Wang, X. Jiang, J. Zhu, Z. Liu, X. Guo, C. Song, A short review of recent advances in CO_2 hydrogenation to hydrocarbons over heterogeneous catalysts, RSC Adv. 8 (2018) 7651–7669, https://doi.org/10.1039/c7ra13546g.
[9] K. Ghaib, K. Nitz, F.-Z. Ben-Fares, Chemical methanation of CO_2: a review, ChemBioEng Rev. 3 (2016) 266–275, https://doi.org/10.1002/cben.201600022.
[10] I. Sreedhar, Y. Varun, S.A. Singh, A. Venugopal, B.M. Reddy, Developmental trends in CO_2 methanation using various catalysts, Catal. Sci. Technol. 9 (2019) 4478–4504, https://doi.org/10.1039/c9cy01234f.
[11] P. Frontera, A. Macario, M. Ferraro, P.L. Antonucci, Supported catalysts for CO_2 methanation: a review, Catalysts 7 (2017) 59, https://doi.org/10.3390/catal7020059.
[12] W. Wang, S. Wang, X. Ma, J. Gong, Recent advances in catalytic hydrogenation of carbon dioxide, Chem. Soc. Rev. 40 (2011) 3703–3727, https://doi.org/10.1039/c1cs15008a.
[13] I. Kuznecova, J. Gusca, Property based ranking of CO and CO_2 methanation catalysts, Energy Procedia 128 (2017) 255–260, https://doi.org/10.1016/j.egypro.2017.09.068.
[14] S. Rönsch, J. Schneider, S. Matthischke, M. Schlüter, M. Götz, J. Lefebvre, P. Prabhakaran, S. Bajohr, Review on methanation — from fundamentals to current projects, Fuel 166 (2016) 276–296, https://doi.org/10.1016/j.fuel.2015.10.111.
[15] F. Fischer, H. Tropsch, P. Dilthey, Reduction of carbon monoxide to methane in the presence of various metals, Brennstoff-Chemie 6 (1925) 265.
[16] M.A. Vannice, The catalytic synthesis of hydrocarbons from carbon monoxide and hydrogen, Catal. Rev. 14 (1976) 153–191, https://doi.org/10.1080/03602457608073410.
[17] G.A. Mills, F.W. Steffgen, Catalytic methanation, Catal. Rev. 8 (1974) 159–210, https://doi.org/10.1080/01614947408071860.
[18] F. Ocampo, B. Louis, L. Kiwi-Minsker, A.C. Roger, Effect of Ce/Zr composition and noble metal promotion on nickel based $Ce_xZr_{1-x}O_2$ catalysts for carbon dioxide methanation, Appl. Catal. A Gen. 392 (2011) 36–44, https://doi.org/10.1016/j.apcata.2010.10.025.
[19] S. Tada, T. Shimizu, H. Kameyama, T. Haneda, R. Kikuchi, Ni/CeO_2 catalysts with high CO_2 methanation activity and high CH_4 selectivity at low temperatures, Int. J. Hydrogen Energy 37 (2012) 5527–5531, https://doi.org/10.1016/j.ijhydene.2011.12.122.
[20] T.T.M. Nguyen, L. Wissing, M.S. Skjøth-Rasmussen, High temperature methanation: catalyst considerations, Catal. Today 215 (2013) 233–238, https://doi.org/10.1016/j.cattod.2013.03.035.
[21] J. Kirchner, J.K. Anolleck, H. Lösch, S. Kureti, Methanation of CO_2 on iron based catalysts, Appl. Catal. B Environ. 223 (2018) 47–59, https://doi.org/10.1016/j.apcatb.2017.06.025.
[22] Z. Baysal, S. Kureti, CO_2 methanation on Mg-promoted Fe catalysts, Appl. Catal. B Environ. 262 (2020) 118300, , https://doi.org/10.1016/j.apcatb.2019.118300.
[23] M. dar Lee, J. fu Lee, C. shang Chang, Catalytic behavior and phase composition change of iron catalyst in hydrogenation of carbon dioxide, J. Chem. Eng. Japan 23 (1990) 130–136, https://doi.org/10.1252/jcej.23.130.
[24] M. Iglesias G, C. De Vries, M. Claeys, G. Schaub, Chemical energy storage in gaseous hydrocarbons via iron Fischer-Tropsch synthesis from H_2/CO_2—kinetics, selectivity and process considerations, Catal. Today 242 (2015) 184–192, https://doi.org/10.1016/j.cattod.2014.05.020.
[25] A.P. Steynberg, R.L. Espinoza, B. Jager, A.C. Vosloo, High temperature Fischer-Tropsch synthesis in commercial practice, Appl. Catal. A Gen. 186 (1999) 41–54, https://doi.org/10.1016/S0926-860X(99)00163-5.
[26] J.X. Liu, P. Wang, W. Xu, E.J.M. Hensen, Particle size and crystal phase effects in fischer-tropsch catalysts, Engineering 3 (2017) 467–476, https://doi.org/10.1016/J.ENG.2017.04.012.
[27] Y. Liu, J.F. Chen, Y. Zhang, The effect of pore size or iron particle size on the formation of light olefins in Fischer-Tropsch synthesis, RSC Adv. 5 (2015) 29002–29007, https://doi.org/10.1039/c5ra02319j.
[28] J.Y. Park, Y.J. Lee, P.K. Khanna, K.W. Jun, J.W. Bae, Y.H. Kim, Alumina-supported iron oxide nanoparticles as Fischer-Tropsch catalysts: effect of particle size of iron oxide, J. Mol. Catal. A Chem. 323 (2010) 84–90, https://doi.org/10.1016/j.molcata.2010.03.025.
[29] H.M. Torres Galvis, J.H. Bitter, T. Davidian, M. Ruitenbeek, A.I. Dugulan, K.P. De Jong, Iron particle size effects for direct production of lower olefins from synthesis gas, J. Am. Chem. Soc. 134 (2012) 16207–16215, https://doi.org/10.1021/ja304958u.
[30] Q. Yang, X.P. Fu, C.J. Jia, C. Ma, X. Wang, J. Zeng, R. Si, Y.W. Zhang, C.H. Yan, Structural determination of catalytically active subnanometer Iron oxide clusters, ACS Catal. 6 (2016) 3072–3082, https://doi.org/10.1021/acscatal.6b00328.
[31] S. He, C. Li, H. Chen, D. Su, B. Zhang, X. Cao, B. Wang, M. Wei, D.G. Evans, X. Duan, A surface defect-promoted Ni nanocatalyst with simultaneously enhanced activity

and stability, Chem. Mater. 25 (2013) 1040–1046, https://doi.org/10.1021/cm303517z.
[32] C. Vogt, E. Groeneveld, G. Kamsma, M. Nachtegaal, L. Lu, C.J. Kiely, P.H. Berben, F. Meirer, B.M. Weckhuysen, Unravelling structure sensitivity in CO_2 hydrogenation over nickel, Nat. Catal. 1 (2018) 127–134, https://doi.org/10.1038/s41929-017-0016-y.
[33] T. Ryu, Y. Kang, I.S. Nam, S.B. Hong, Iron-exchanged high-silica LTA zeolites as hydrothermally stable NH_3-SCR catalysts, React. Chem. Eng. 4 (2019) 1050–1058, https://doi.org/10.1039/c9re00007k.
[34] F. Gao, Y. Zheng, R.K. Kukkadapu, Y. Wang, E.D. Walter, B. Schwenzer, J. Szanyi, C.H.F. Peden, Iron loading effects in Fe/SSZ-13 NH_3-SCR catalysts: nature of the Fe ions and structure-function relationships, ACS Catal. 6 (2016) 2939–2954, https://doi.org/10.1021/acscatal.6b00647.
[35] N. Martín, P.N.R. Vennestrøm, J.R. Thøgersen, M. Moliner, A. Corma, Iron-containing SSZ-39 (AEI) zeolite: an active and stable high-temperature NH_3-SCR catalyst, ChemCatChem 9 (2017) 1754–1757, https://doi.org/10.1002/cctc.201601627.
[36] M.C. Bacariza, I. Graça, J.M. Lopes, C. Henriques, Tuning zeolite properties towards CO_2 methanation: an overview, ChemCatChem 11 (2019) 2388–2400, https://doi.org/10.1002/cctc.201900229.
[37] M.C. Bacariza, R. Bértolo, I. Graça, J.M. Lopes, C. Henriques, The effect of the compensating cation on the catalytic performances of Ni/USY zeolites towards CO_2 methanation, J. CO_2 Util. 21 (2017) 280–291, https://doi.org/10.1016/j.jcou.2017.07.020.
[38] M.C. Bacariza, I. Graça, J.M. Lopes, C. Henriques, Enhanced activity of CO_2 hydrogenation to CH_4 over Ni based zeolites through the optimization of the Si/Al ratio, Microporous Mesoporous Mater. 267 (2018) 9–19, https://doi.org/10.1016/j.micromeso.2018.03.010.
[39] M.C. Bacariza, M. Maleval, I. Graça, J.M. Lopes, C. Henriques, Power-to-methane over Ni/zeolites: influence of the framework type, Microporous Mesoporous Mater. 274 (2019) 102–112, https://doi.org/10.1016/j.micromeso.2018.07.037.
[40] R. Delmelle, R.B. Duarte, T. Franken, D. Burnat, L. Holzer, A. Borgschulte, A. Heel, Development of improved nickel catalysts for sorption enhanced CO_2 methanation, Int. J. Hydrogen Energy 41 (2016) 20185–20191, https://doi.org/10.1016/j.ijhydene.2016.09.045.
[41] A. Borgschulte, N. Gallandat, B. Probst, R. Suter, E. Callini, D. Ferri, Y. Arroyo, R. Erni, H. Geerlings, A. Züttel, Sorption enhanced CO_2 methanation, Phys. Chem. Chem. Phys. 15 (2013) 9620–9625, https://doi.org/10.1039/c3cp51408k.
[42] S. Walspurger, G.D. Elzinga, J.W. Dijkstra, M. Sarić, W.G. Haije, Sorption enhanced methanation for substitute natural gas production: experimental results and thermodynamic considerations, Chem. Eng. J. 242 (2014) 379–386, https://doi.org/10.1016/j.cej.2013.12.045.
[43] F. Massa, A. Coppola, F. Scala, A thermodynamic study of sorption-enhanced CO_2 methanation at low pressure, J. CO_2 Util. 35 (2019) 176–184, https://doi.org/10.1016/j.jcou.2019.09.014.
[44] R. Delmelle, J. Terreni, A. Remhof, A. Heel, J. Proost, A. Borgschulte, Evolution of water diffusion in a sorption-enhanced methanation catalyst, Catalysts 8 (2018) 341, https://doi.org/10.3390/catal8090341.
[45] J. Rouquerol, P. Llewellyn, F. Rouquerol, Is the BET equation applicable to microporous adsorbents? in: P.L. Llewellyn, F. Rodriquez-Reinoso, J. Rouqerol, N. Seaton (Eds.), Studies in Surface Science and Catalysis, Elsevier, 2007, pp. 49–56, , https://doi.org/10.1016/s0167-2991(07)80008-5.
[46] J. Zieliński, I. Zglinicka, L. Znak, Z. Kaszkur, Reduction of Fe_2O_3 with hydrogen, Appl. Catal. A Gen. 381 (2010) 191–196, https://doi.org/10.1016/j.apcata.2010.04.003.
[47] S.S.R. Putluru, L. Schill, A.D. Jensen, R.S.N. Fehrmann, Selective catalytic reduction of NO_x with NH_3 on Cu-, Fe-, and Mn-Zeolites prepared by impregnation: comparison of activity and hydrothermal stability, J. Chem. 2018 (2018) 1–11, https://doi.org/10.1155/2018/8614747.